frontiers in Energy Research

ORIGINAL RESEARCH
published: 12 February 2021
doi: 10.3389/fenrg.2020.615558

Preparation and Electrochemical Performance of V_2O_5 @N-CNT/S Composite Cathode Materials

Cheng Liu[1], Meng Xiang[1], Haiyang Zhang[1], Shuaiqiang Feng[1], Jianrong Xiao[1,2], Songshan Ma[2] and Xinyu Li[1]**

[1]College of Science, Guilin University of Technology, Guilin, China, [2]School of Physics and Electronics, Central South University, Changsha, China*

Lithium–sulfur battery hasreceived widespread attention because of its high energy density, low cost, environmental friendliness, and nontoxicity. However, the insulating properties of elemental sulfur, huge volume changes, and dissolution of polysulfides in electrolytes that result in the shuttle effect, low sulfur utilization, and low rate performance seriously hinder the commercialization of lithium–sulfur batteries. In this work, a composite material of nitrogen-doped multiwalled carbon nanotubes and V_2O_5 was designed and fabricated to serve as the positive electrode of lithium–sulfur battery via the hydrothermal method. The positive electrode of the V_2O_5@N-CNTs composite material could reach an initial discharge specific capacity of 1,453 mAh g^{-1}at a rate of 0.1C. Moreover, the composite material could maintain a discharge ratio of 538 mAh g^{-1} at a rate of 0.5C even after 200 charge and discharge cycles. After 400 cycles, the composite had a specific discharge capacity of 439 mAh g^{-1} at a rate of 1.0C. The excellent electrochemical performance of the V_2O_5@N-CNT/S composite cathode material was due to the fact that V_2O_5 contains oxygen ions and has a strong polarized surface. Furthermore, nitrogen doping changed the hybrid structure of carbon atoms and provided additional active sites, thereby improving the conductivity of the material itself and effectively inhibiting the dissolution and diffusion of polysulfides.

Keywords: lithium–sulfur battery, multiwalled carbon nanotubes, V_2O_5, nitrogen doping, cycle performance

OPEN ACCESS

Edited by:
Xingxing Gu,
Chongqing Technology and Business University, China

Reviewed by:
Tiefeng Liu,
Zhejiang University of Technology, China
Terence Liu,
Northumbria University, United Kingdom

****Correspondence:***
Jianrong Xiao
xjr@glut.edu.cn
Xinyu Li
lixinyu5260@163.com

Speciality section:
This article was submitted to Electrochemical Energy Conversion and Storage, a section of the journal Frontiers in Energy Research

Received: *09 October 2020*
Accepted: *29 October 2020*
Published: *12 February 2021*

Citation:
Liu C, Xiang M, Zhang H, Feng S, Xiao J, Ma S and Li X (2021) Preparation and Electrochemical Performance of V_2O_5 @N-CNT/S Composite Cathode Materials. Front. Energy Res. 8:615558. doi: 10.3389/fenrg.2020.615558

INTRODUCTION

Lithium-ion batteries are widely used in energy storage and portable electronic device applications (Goodenough and Park, 2013; Wu et al., 2018; Yang et al., 2018a; Yang et al., 2018b; Zhang et al., 2018; Leng et al., 2019; Ye et al., 2019). However, the application of lithium-ion batteries in electric vehicles is limited because of their low theoretical energy density. Lithium–sulfur batteries have received increased attention because of their high energy density, low cost, environmental friendliness, and nontoxicity (Yuan et al., 2016; Wu et al., 2019a; Gu et al., 2020; Zhang et al., 2020). Nevertheless, the insulation of elemental sulfur, huge volume changes, and dissolution of polysulfides in electrolytesthat result in the shuttle effect, low sulfur utilization, and low rate performance seriously hinder the commercialization of lithium–sulfur batteries (Peng et al., 2017; Zhang et al., 2017; He et al., 2018; Gu and Lai, 2019; Zhu et al., 2019).

The electrochemical performance of lithium–sulfur batteries can be improved to solve polysulfide dissolution and diffusion. Various cathode materials, such as carbon nanotubes (CNTs), conductive

polymers, and metal compounds, are widely used in lithium–sulfur batteries (Chen et al., 2017; Guo et al., 2017; Zeng et al., 2017; Gu et al., 2019; Wu et al., 2019b). Carbon materials, carbon nanofibers, porous carbon, and grapheneare used and applied as sulfur host materials because of their large specific surface area, high conductivity, and suitable pore size (Balach et al., 2015; Kong et al., 2018; Yang et al., 2018c; Zhao et al., 2018; Yang et al., 2019). Nevertheless, the van der Waals interaction between carbon materials and polysulfides is a weak force and cannot effectively inhibit the shuttle effect. Polar materials can effectively increase polysulfide adsorption via strong chemical bonds, thereby reducing the dissolution and shuttle of polysulfides. Numerous studies on various polar materials, such as TiO_2, MnO_2, SiO_2, and V_2O_5 have been conducted (Liu et al., 2017; Xue et al., 2017; Lin et al., 2018; Tang et al., 2018; An et al., 2019; Tong et al., 2019; Wang et al., 2019; Qin et al., 2020). Moreover, Yuan et al. found that transition metal phosphides can not only capture soluble polysulfides, but also effectively catalyze the decomposition of Li_2S, which improve the utilization of active materials and cycle performance (Yuan et al., 2017). However, the conductivity of polar materials is generally lower than that of nanocarbon host materials, resulting in lower sulfur utilization and rate performance. Therefore, highly conductive and strongly adsorbing polar compound host materials combined with nanocarbon must be developed to increase electrical conductivity, improve electrolyte contact, and provide more effective chemical and physical constraints on polysulfides, thus improving battery performance (Hong et al., 2018; Li et al., 2018).

Multiwalled CNTs (MWCNTs) are extensively utilized in energy storage materials because of their high structural stability and good electronic conductivity. Razzaq et al. (2019) prepared thin-film composites with CNTs as the main chain via electrospinning; these composites exhibited excellent cycle performance on the positive electrode of lithium–sulfur batteries. Other researchers adopted solid-state growth strategies for preparing highly nitrogen-doped graphene and carbon tube composite cathode materials with a 3D structure; Yuan et al. synthesized nitrogen-doped nanoparticles with a coordinated nitrogen structure and a controllable concentration. Pyridine nitrogen-doped carbon not only shows the strongest lithium polysulfide trapping ability, but also can accelerate the conversion of Li_2S. The cathode based on pyridine nitrogen-doped carbon has higher capacity and better cycle stability (Yuan et al., 2018). Their studies proved that the introduction of nitrogen atoms can change the hybrid structure of carbon atoms to increase the conductivity of the composite material and the adsorption of polysulfides (Ding et al., 2016; Chen et al., 2018; Yin et al., 2018; Fan et al., 2019; Fang et al., 2019) . Several works fabricated CNTs whose surfaces are coated with V_2O_5 of different thicknesses; their bonding point is located on the surface of the CNTs. Coating with V_2O_5 effectively inhibits the shuttle of polysulfides and improves sulfurutilization (Carter et al., 2017). Given that MWCNTs have high conductivity and polar metal oxides have excellent adsorption and catalytic abilities, their interwoven conductive network structure can quickly transfer electrons, and the 3D network structure that they form provide greater adsorption for sulfur point (Wang et al., 2016).

In this study, a combination of a polar metal oxide, namely, V_2O_5, and nitrogen-doped MWCNTs was used as the sulfur host material. A nitrogen-doped 3D conductive network structure, namely, MWCNT/V_2O_5/S composite cathode, was prepared via simple melting and hydrothermal synthesis methods. The preparation process is uncomplicated, and the conductive network structure of MWCNTs can absorb V_2O_5 nanoparticles well.

EXPERIMENT

Material Preparation

Preparation of nitrogen-doped V_2O_5/MWCNTs: NH_3VO_4 powder was calcined in air at 350°C for 2 h to obtain V_2O_5 powder. Carbon tubes and urea were uniformly mixed at a ratio of 1:10 and then placed onto the lining of a 100 ml reactor. The mixture was hydrothermally reacted at 200°C for 12 h. The mixture was repeatedly centrifuged with deionized water and absolute ethanol to obtain nitrogen-doped MWCNTs (N-MWCNTs). Subsequently, 0.2 g of the V_2O_5 powder was added to a suspension containing 0.3 g of N-MWCNTs, and then it was ultrasonicated for 30 min. The sonicated aqueous solution was vacuum-filtered with deionized water, dried in an oven at 60°C for 12 h, and completely and uniformly ground to obtain the composite material, namely, V_2O_5/N-MWCNT.

Preparation of V_2O_5/MWCNTs: V_2O_5/MWCNTs and sulfur were placed in an agate mortar at a ratio of 3:7 and evenly ground. The ground material was put into a glove box to remove oxygen, and then it was put onto the lining of a 25 ml reactor. Finally, it was melted in an oven at 155°C for 12 h to obtain a composite material loaded with sulfur. V_2O_5/MWCNT/S and MWCNT/S composite materials doped with nitrogen were obtained via the same method and at the same ratio.

Material Characterization and Analysis

The micro morphologies of the composite materials were examined via scanning electron microscopy (SEM, HITACHIS-4800). Excitation voltage was set to 5 kV, and relative pressure (P/P0) was set to 0.05–0.2. The crystal structures of the materials were analyzed via X-ray diffraction (XRD, MiniFlex-600) by using Cu–Ka as the radiation source at a scanning rate of 20 min^{-1}, cavity voltage of 40 kV, and tube current of 30 mA. The elemental compositions of the composite materialswere measured via X-ray energy spectrometry (EDS, S-00123). The electronic binding energies of the V_2O_5/N-MWCNT/S composite materials were measured via X-ray photoelectron spectroscopy (XPS, Escalab-250XI) to determine element valence distributions and bonding modes. Raman spectra under argon ion laser excitation were characterized using a Thermo Fisher-DXR system. The sulfur contents of the composite materials were detected via TGA analysis within the temperature range of 400–700°C at a heating rate of 20°C/min.

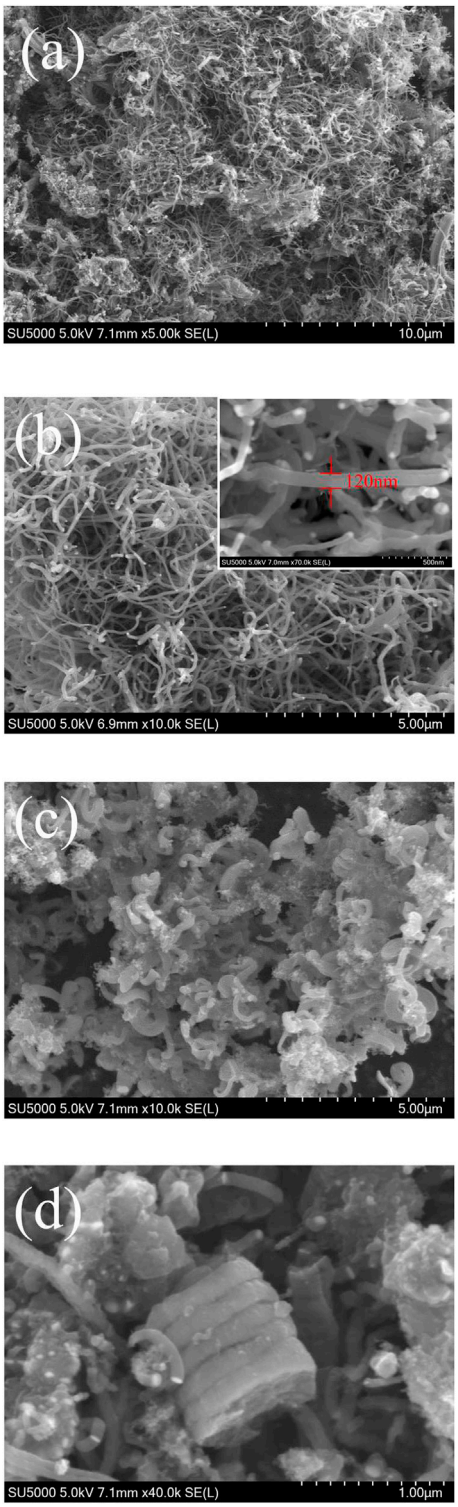

FIGURE 1 | (A,B) SEM images of MWCNTs at different magnifications. **(C)** SEM images of the V_2O_5/MWCNT composite material. **(D)** SEM images of the nitrogen-doped V_2O_5/MWCNT composite material.

Electrochemical Performance Test

Theactive materials, namely, Super P (conductive agent) and polyvinylidene fluoride (battery-grade binder),were uniformly mixed in N-methylpyrrolidone ata mass ratio of 7:2:1. The active materials were uniformly coated onto an aluminum foil via the doctor blade coating technology, and sulfur loading was 1.1 mg cm^{-2}. Pole pieces were dried in an oven at 60°C for 12 h, cut into positive pole pieces with a diameter of 16 mm, and then assembled into a button cell (CR 2025). The contents of O_2 and H_2O in the glove box were strictly controlled to less than 0.1 ppm, and the prepared electrode sheet was used as the positive electrode. A Celgard 2,400 polypropylene microporous membrane was used. A metal lithium sheet served as the negative electrode. The electrolyte type was LS-002 type. The main components were 1,3-dioxolane and 1,2-dimethoxyethane (at a volume ratio of 1:1) containing a 1 wt% $LiNO_3$ additive. The top–down assembly sequence was completed in the order of positive electrode shell, positive electrode sheet, electrolyte, separator, metal lithium sheet, foamed nickel, and negative electrode shell. The assembled battery was left to stand overnight for 12 h, and a BTS battery test system (Neware BTS 7.0) was used for the relevant electrochemical performance tests at a constant temperature of 25°C. The ratio of electrolyte to sulfur is 20 μl mg^{-1}.

RESULTS AND DISCUSSION

The MWCNTs consisted of numerous closely intertwined CNTs that formed a 3D conductive network structure (**Figures 1A**,**B**). The diameter of the carbon tubes was about 120 nm. This 3D network structure could tightly wrap the sulfur particles, and the internal 3D network space structure could hold large amounts of the active substances. Thus, these structures effectively alleviated the problem of sulfur volume expansion. The length of the MWCNTs could be extended from tens to hundreds of nanometers (**Figure 1C**), thus effectively improving the overall conductivity of the composite materials. The V_2O_5 particles loaded onto the surface of the MWCNTs not only promoted the rapid transmission of lithium ions but also exerted a certain catalytic effect, thereby accelerating the conversion process of the intermediate product lithium polysulfide. Simultaneously, the higher structural stability of the 3D network constructed by the MWCNTs effectively inhibited polysulfide dissolution and diffusion. The V_2O_5/MWCNT/S composite material after nitrogen doping is shown in **Figure 1D**. The morphology of the composite materials after nitrogen doping did not evidently change compared with that before nitrogen doping. Therefore, the composite materials were further analyzed using an elemental energy spectrometer. The EDS mapping of the samples corresponding to C, N, O, V, and S elements is shown in **Figure 2**. The overall

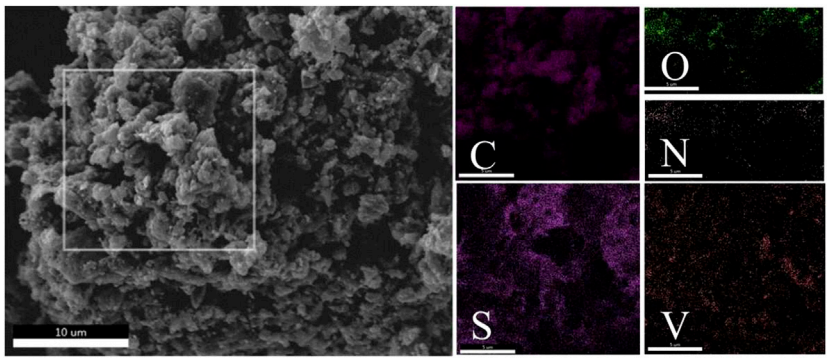

FIGURE 2 | SEM images of the nitrogen-doped V_2O_5/MWCNT/S composite materials, and EDS spectrum of the nitrogen-doped V_2O_5/S composite material.

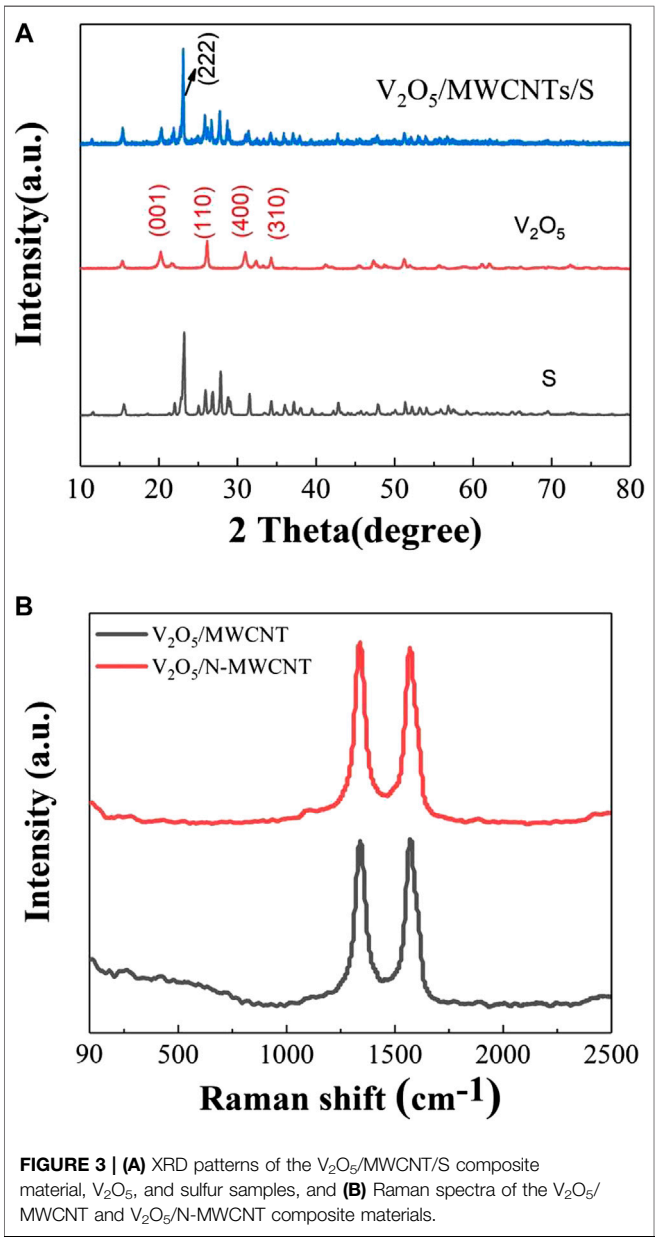

FIGURE 3 | (A) XRD patterns of the V_2O_5/MWCNT/S composite material, V_2O_5, and sulfur samples, and **(B)** Raman spectra of the V_2O_5/MWCNT and V_2O_5/N-MWCNT composite materials.

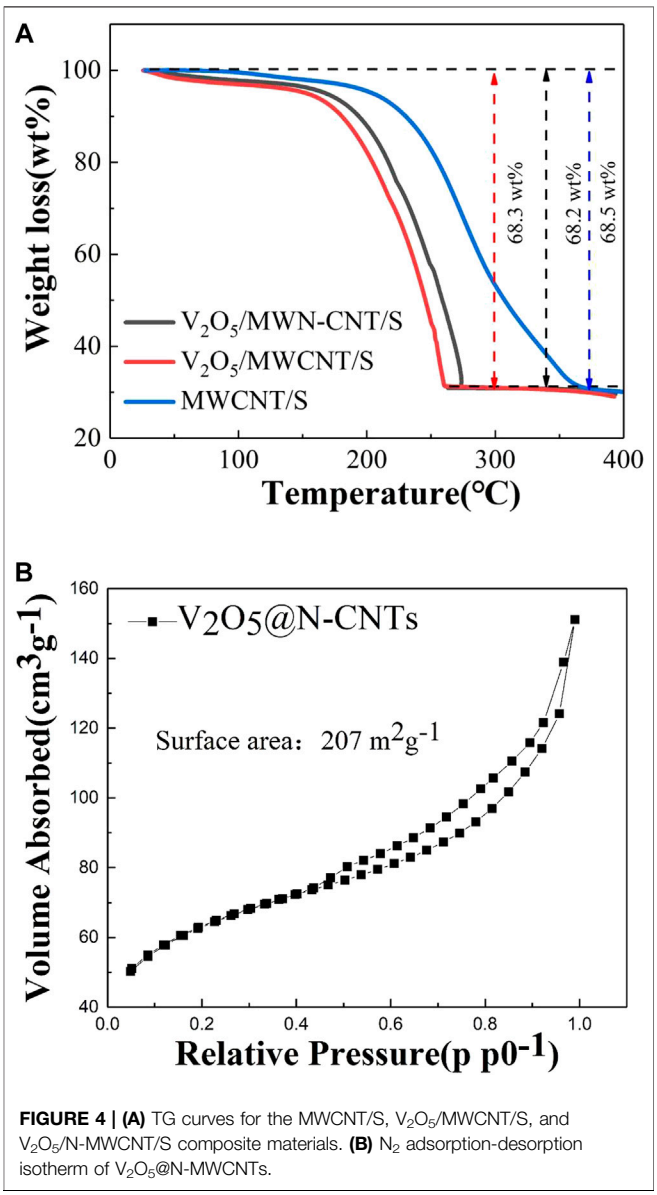

FIGURE 4 | (A) TG curves for the MWCNT/S, V_2O_5/MWCNT/S, and V_2O_5/N-MWCNT/S composite materials. **(B)** N_2 adsorption-desorption isotherm of V_2O_5@N-MWCNTs.

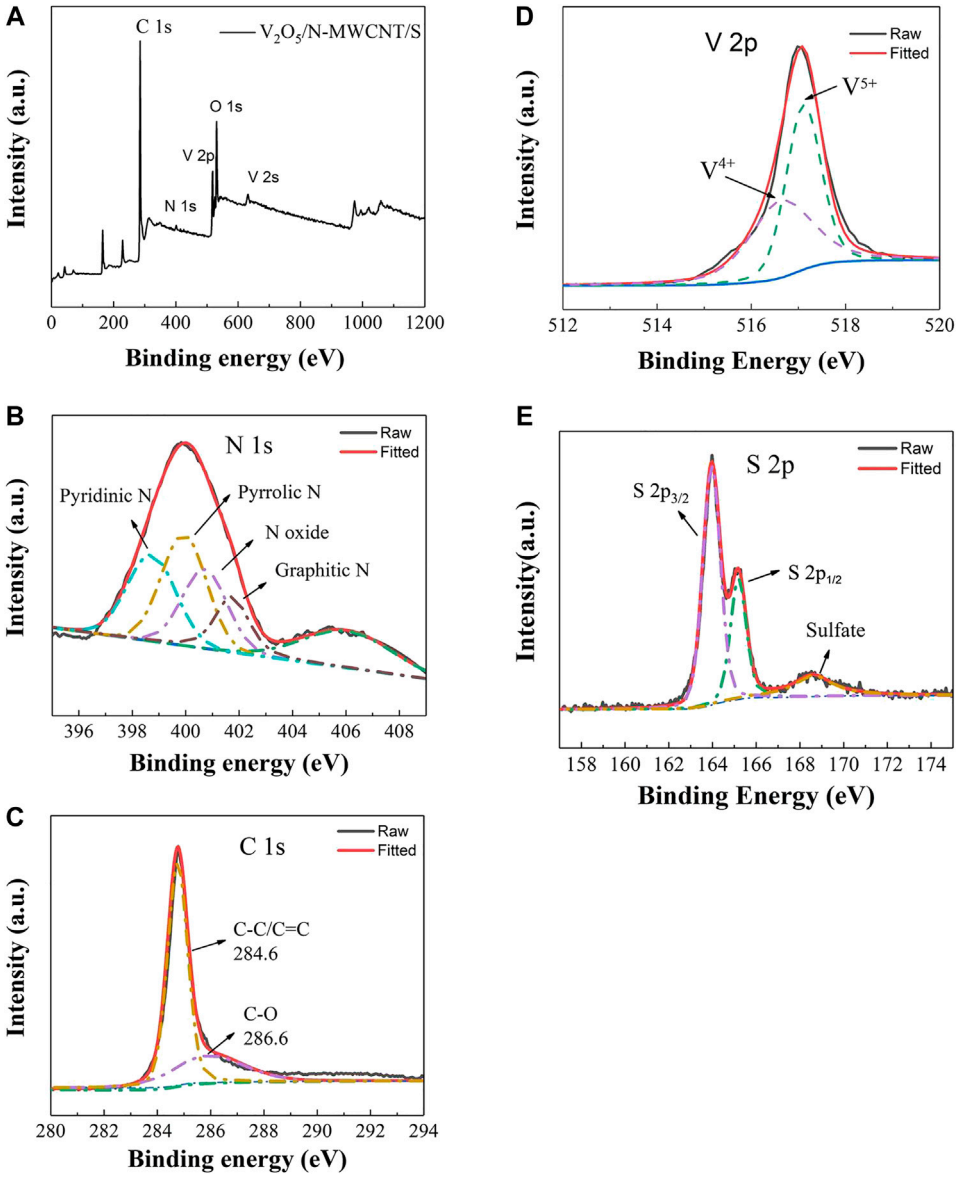

FIGURE 5 | (A) XPS full scan spectra of V_2O_5/N-MWCNT/S. **(B)** High-resolution N 1 s, **(C)** C 1 s, **(D)** V2p, and **(E)** S2p XPS spectra of the V_2O_5/N-MWCNT/S composite material.

elemental distribution was relatively uniform. The presence of nitrogen could also be clearly observed, indicating that nitrogen was successfully doped into the V_2O_5/MWCNT/S samples via the hydrothermal method. Although the overall nitrogen content was relatively small, its distribution was relatively uniform. The introduction of nitrogen played a certain role in increasing the conductivity and adsorption of the composite materials.

The diffraction patterns of S, V_2O_5, and V_2O_5/MWCNT/S samples are depicted in **Figure 3A**, which shows that the composite sample retained the diffraction characteristic peaks of V_2O_5 that corresponded to the (001), (110), (400), and (310) crystal planes. At 23.1°, the strongest characteristic peak of sulfur was still maintained in the composite materials, and this peak corresponded to the characteristic peak of the typical S_8 bond structure. The Raman spectra of the V_2O_5/MWCNT and V_2O_5/N-MWCNT composite materials are shown in **Figure 3B**. The D and G peaks of graphite could be observed at 1,350 and 1,590 cm^{-1} (Hou et al., 2016). Peak D indicated the presence of crystal defects in carbon atoms, whereas peak G denoted sp^3 hybridization. The values of the V_2O_5/MWCNT and V_2O_5/N-MWCNT composite materials were 1.00 and 1.02, respectively. Results demonstrated that the nitrogen-doped MWCNTs had a greater degree of defects and were more conducive to electron conduction, thus increasing the cycle efficiency of

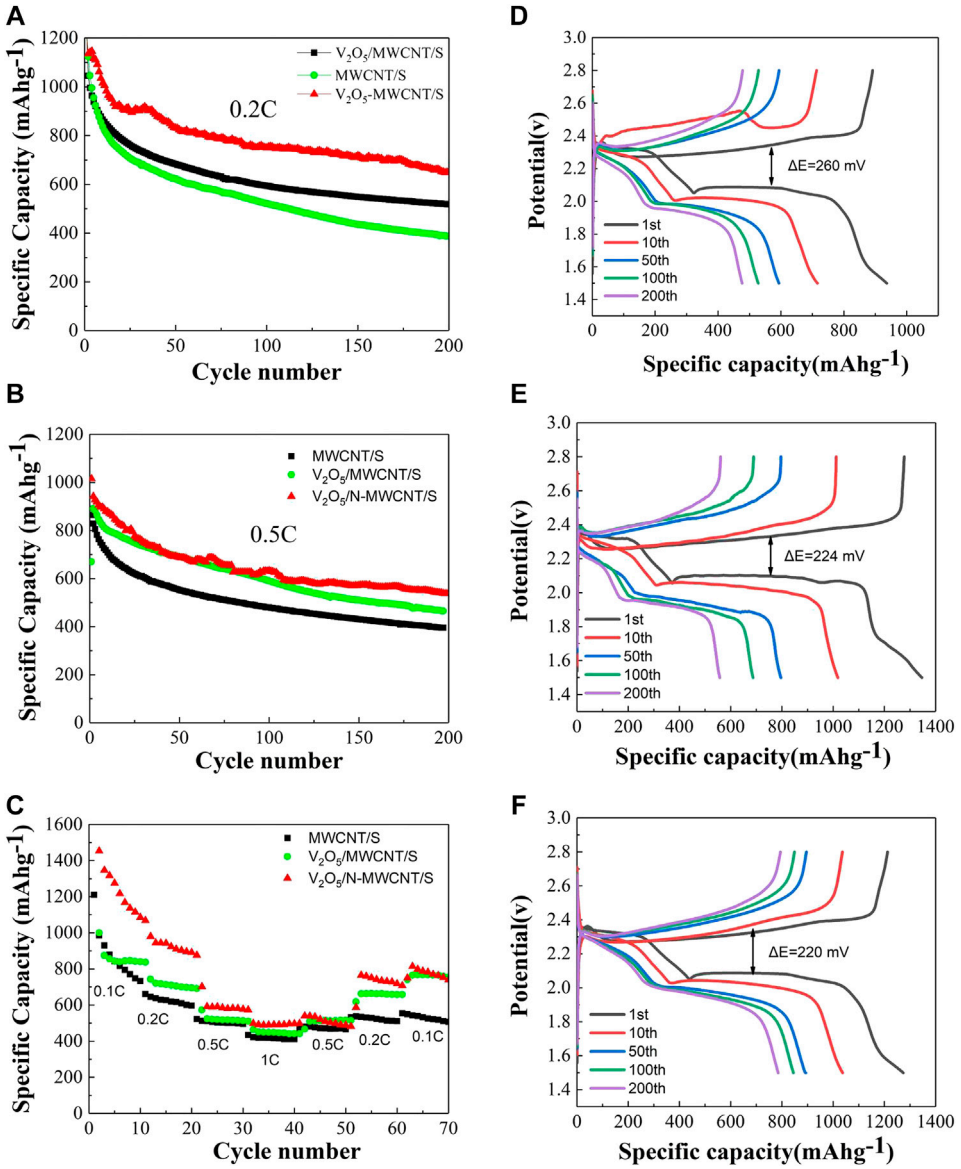

FIGURE 6 | (A–C) Cycle performance of the V_2O_5/N-MWCNT/S, V_2O_5/MWCNT/S, and MWCNT/S composite materials at 0.2, 0.5, and 1 C **(D–F)** Cycle performance of the MWCNT/S, V_2O_5/MWCNT/S, and V_2O_5/N-MWCNT/S composite materials at 0.1 C within 1.5–3.0 V from the 1st to the 200th discharge and charge curves.

the lithium–sulfur battery (Hou et al., 2016; Ma et al., 2017). The thermogravimetric diagrams of the samples are shown in **Figure 4**. The weight loss of the MWCNT/S, V_2O_5/MWCNT/S, and V_2O_5/N-MWCNT/S composite materials was 68.3, 68.2, and 68.5%, respectively, indicating that the MWCNTs supported a higher sulfur content while providing more active sites.

The chemical composition of the structure of the V_2O_5/N-MWCNT/S composite material was analyzed via XPS. **Figure 5A** shows the C, N, O, V, and other elements in the V_2O_5/N-MWCNT/Scomposite material. N peak could be clearly observed, indicating that nitrogen was successfully doped into the CNTs. The peak positions of V2p and V2s corresponded to about 517 and 630 eV, respectively. A high-resolution map of nitrogen in the material is displayed in **Figure 5B**. N 1S was fitted via the Gaussian peak splitting method. The four peaks clearly corresponded to pyridine N (398.5 eV), pyrrole N (399.6 eV), oxide N (400.9 eV), and graphite N (402.1 eV). Pyridine N and pyrrole N from urea can introduce more defects, thereby changing the electronic distribution state of charge, providing additional active adsorption sites for polysulfides, and effectively improving the cycle stability of lithium–sulfur batteries (Xiao et al., 2017; Jiang et al., 2018). The two peaks at 284.6 and 286.6 eV were C–C/C=C and C–O, respectively (**Figure 5C**) (Zheng et al., 2017). The XPS peak position of $V2p_{3/2}$ was located at 517.1 eV,

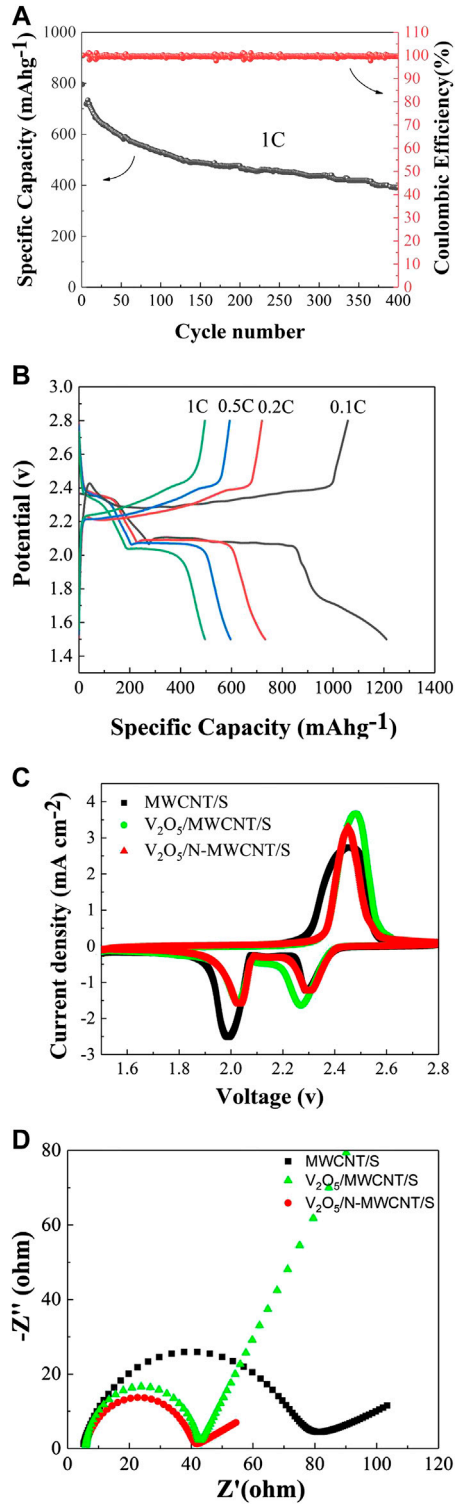

FIGURE 7 | (A) Long cycle performance of the V_2O_5/N-MWCNT/S composite material at 1 **C**. **(B)** Initial charge and discharge curves of the V_2O_5/N-MWCNT/S composite material. **(C)** CV curves of the V_2O_5/N-MWCNT/S, V_2O_5/MWCNT/S, and MWCNT/S composite materials. **(D)** EIS spectra of the V_2O_5/N-MWCNT/S, V_2O_5/MWCNT/S, and MWCNT/S composite materials.

corresponding to the V^{5+} valence state of the V_2O_5 compound (**Figure 5D**). This result proved that the valence of V_2O_5 did not change. The binding energies of 163.9 and 165.1 eV corresponded to the $S2p_{1/2}$ and $S2p_{3/2}$ orbitals, respectively (**Figure 5E**), consistent with the position of the binding energy peak of elemental sulfur reported in the literature (Wang et al., 2014; Li et al., 2016).

Whenthe V_2O_5@MWCNT/S composite material was charged and discharged at a rate of 0.2°C, the first discharge specific capacity could reach 1,257 mAh g^{-1} (**Figure 6A**). Even after 200 cycles, the discharge specific capacity was still 518 mAh g^{-1}. Therefore, the cycle performance of the V_2O_5@MWCNTs/S composite material was better than that of the MWCNT/S composite material. Similarly, when charging and discharging at a rate of 0.5C, the specific capacity of the nitrogen-doped V_2O_5/MWCNT/S composite material could reach 538 mAh g^{-1} even after 200 cycles, and its overall cycle performance was also better than that of the V_2O_5/MWCNT/S (465 mAh g^{-1}) and MWCNT/S composite materials (395 mAh g^{-1}) (**Figure 6B**). In terms of rate performance, the overall performance of the V_2O_5/N-MWCNT/S composite material was also better than that of the MWCNT/S composite material (**Figure 6C**). The excellent rate performance of the V_2O_5/N-MWCNT/S composite material was due to the 3D conductive network system constructed by V_2O_5 and MWCNTs. Nitrogen doping effectively improved the conductivity of carbon and its chemical adsorption capacity for lithium polysulfide. Moreover, V_2O_5 promoted the rapid transfer of electrons in the intermediate polysulfide. The charge–discharge cycle curves of different samples at a rate of 0.1C are exhibited in **Figures 6D–F**. The two obvious discharge platforms at 2.1 and 2.3 V were clearly similar to the multistep conversion process of sulfur. The charge–discharge platform at 2.3 V was relatively stable, transforming sulfur into long-chain polysulfides; at 2.1 V, the other stable segment belonged to short-chain polysulfides that further transformed into Li_2S_2/Li_2S. The change in charge platform was actually the transition from Li_2S_2/Li_2S to Li_2S_8/S_8. Furthermore, the number of cycles increased, and the potential difference between the charge and discharge curves gradually increased. The polarization potential between the charge and discharge curves of the V_2O_5/MWCNT/S composite material after nitrogen doping was considerably smaller than that of the MWCNT/S and V_2O_5/MWCNT/S composite materials. This result also demonstrated that the positive electrode of the nitrogen-doped V_2O_5/MWCNT/S composite material had better cycle stability and played a certain role in inhibiting the shuttle effect of polysulfides.

After 400 charge and discharge cycles at a rate of 1C, the discharge specific capacity was 439 mAh g^{-1} (**Figure 7A**). The nitrogen-doped V_2O_5/MWCNT/S composite material maintained an excellent cycle performance. The charge and discharge performance curves of the battery at different rates are illustrated in **Figure 7B**. As current density increased, the overall discharge specific capacity of the battery gradually decreased, and the polarization phenomenon between the charge and discharge curves became increasingly serious. Nevertheless, the lithium–sulfur battery still maintained a

TABLE 1 | Comparison of Li-S Battery Performance with different materials.

	Sulfur host	Advantages	Capacity
Yuan et al. (2017)	$N4_M$-C	Strongest capture ability of the lithium polysulfides	1,295, 1,137, 980, 931 mAh g^{-1} at 0.1, 0.2, 0.5, and 1C
Yuan et al. (2018)	Ni_2P@NPC	Trap the soluble polysulfides	1,165, 1,024, 912, 870, and 812 mAh g^{-1} at 0.1 , 0.2 , 0.5 , 1, and 2C
Huang et al., 2020	$FePO_4$@rGO	Physical confinement and chemical interaction to restrict shuttle effect	1,256, 1,116, 997, 810 mAh g^{-1} at 0.1, 0.2, 0.5, 1C
This work	V_2O_5@N-MWCNTs	Porous structure, large specific surface and superior adsorption capacity	1,453, 1,214, 942, and 718 mAh.g^{-1} at 0.1, 0.2, 0.5, 1C

typical charging and discharging platform overall. The cyclic voltammetry characteristic curves of the MWCNT/S and V_2O_5/N-MWCNT/S composite materials are depicted in **Figure 7C**, which shows one oxidation peak and two reduction peaks. The reduction peaks at 2.3 and 2.0 V corresponded to the conversion of S_8 to Li_2S_X ($4 \le x \le 8$) and the conversion of Li_2S_X ($4 \le x \le 8$) to Li_2S_2/Li_2S, respectively. The CV curve also had an oxidation peak at 2.5 V, which corresponded to the conversion reaction of Li_2S_2/Li_2S to Li_2S_X ($4 \le x \le 8$) and S8. The oxidation peak potential of the V_2O_5/MWCNT/S composite material was lower and its reduction peak potential was higher than that of the MWCNT/S composite material. This observation also indicated that the V_2O_5/MWCNT/S composite material had a lower oxidation and a higher reduction potential than the other composite materials. In addition, the polar metal oxide (V_2O_5) accelerated the kinetic conversion process, and the synergy of V_2O_5 and MWCNTs also played a certain role in improving the cycle stability of the lithium–sulfur battery. After the Z-view software was fitted, the charge transfer resistance of the nitrogen-doped V_2O_5/MWCNT/S became smaller after the cycle, also indicating that the charge transfer ability of the composite sample was stronger (**Figure 7D**). **Table 1** is demonstrated according to the different materials of Li-S batteries performance.

CONCLUSION

In this work, MWCNTs were doped with nitrogen via the hydrothermal reduction method. V_2O_5 nanoparticles were attached onto the surface of the MWCNTs and combined with sulfur (i.e., MWCNT/S) to prepare battery cathode materials. The 3D conductive network structure constructed by the MWCNTs accelerated electron transfer. The polar metal oxide, i.e., V_2O_5, had greater chemical adsorption and catalytic abilities that allowed it to accelerate the entire kinetic reaction process. The hybrid structure of carbon atoms changed, polysulfide adsorption improved, and the dissolution and diffusion of polysulfides were effectively inhibited by using the nitrogen source provided by urea to introduce more defects. Under the synergistic effects of V_2O_5 and MWCNTs, the overall electrochemical performance of the composite cathode materials was effectively enhanced. The initial discharge specific capacity could reach 1,453 mAh g^{-1} at a rate of 0.1C, and a high discharge specific capacity of 538 mAh g^{-1} was maintained even after 200 charge and discharge cycles at a rate of 0.5C. The capacity retention rate was 60%. At a rate of 1.0C, the composite material still had a specific discharge capacity of 492 mAh g^{-1} even after 400 charge and discharge cycles. The excellent cycle performance of the composite material was mainly due to the effective binding of V_2O_5 to polysulfides that reduced the further dissolution of the active substances. The improvement in the rate performance of the V_2O_5/N-MWCNT composite material was due to the stable and efficient 3D conductive network system built by the nitrogen-doped MWCNTs. This structure provided numerous active adsorption sites for sulfur and effectively improved the utilization of the active materials. The conductive 3D network structure that formed exhibited good electrochemical performance. This result offers a promising prospect for developing lithium–sulfur batteries.

DATA AVAILABILITY STATEMENT

The original contributions presented in the study are included in the article/Supplementary Material, further inquiries can be directed to the corresponding authors.

AUTHOR CONTRIBUTIONS

CL, MX, and HZ wrote the draft. JX and XL conceived the idea. SF and SM contributed to the investigation on the related references. All authors contributed to the discussion.

FUNDING

The authors would like to acknowledge financial support provided by Guangxi Key Laboratory of Electrochemical and Magneto chemical Functional Materials Open Foundation (No. EMFM20182203).

REFERENCES

An, C., Yuan, Y., Zhang, B., Tang, L., Xiao, B., He, Z., et al. (2019). Graphene wrapped FeSe 2 nano-microspheres with high pseudocapacitive contribution for enhanced Na-ion storage. *Adv. Energy Mater.* 9, 1900356. doi:10.1002/aenm.201900356

Balach, J., Jaumann, T., Klose, M., Oswald, S., Eckert, J., and Giebeler, L. (2015). Functional mesoporous carbon-coated separator for long-life, high-energy lithium-sulfur batteries. *Adv. Funct. Mater.* 25, 5285–5291. doi:10.1002/adfm.201502251

Carter, R., Oakes, L., Muralidharan, N., Cohn, A. P., Douglas, A., and Pint, C. L. (2017). Polysulfide anchoring mechanism revealed by atomic layer deposition of V2O5 and sulfur-filled carbon nanotubes for lithium-sulfur batteries. *ACS Appl. Mater. Interfaces.* 9, 7185–7192. doi:10.1021/acsami.6b16155

Chen, M., Lu, Q., Jiang, S., Huang, C., Wang, X., Wu, B., et al. (2018). MnO2 nanosheets grown on the internal/external surface of N-doped hollow porous carbon nanospheres as the sulfur host of advanced lithium-sulfur batteries. *Chem. Eng. J.* 335, 831–842. doi:10.1016/j.cej.2017.11.039

Chen, T., Ma, L., Cheng, B., Chen, R., Hu, Y., Zhu, G., et al. (2017). Metallic and polar Co 9 S 8 inlaid carbon hollow nanopolyhedra as efficient polysulfide mediator for lithium−sulfur batteries. *Nano Energy.* 38, 239–248. doi:10.1016/j.nanoen.2017.05.064

Ding, Y.-L., Kopold, P., Hahn, K., van Aken, P. A., Maier, J., and Yu, Y. (2016). Facile solid-state growth of 3D well-interconnected nitrogen-rich carbon nanotube-graphene hybrid architectures for lithium-sulfur batteries. *Adv. Funct. Mater.* 26, 1112–1119. doi:10.1002/adfm.201504294

Fan, X., Tan, F., Meng, F., and Liu, J. (2019). Hierarchical porous N-doped carbon nanosheets obtained by organic-inorganic bipolymeric engineering for improved lithium-sulfur batteries. *Chem. Eur J.* 25, 4040–4046. doi:10.1002/chem.201805803

Fang, D., Wang, Y., Qian, C., Liu, X., Wang, X., Chen, S., et al. (2019). Synergistic regulation of polysulfides conversion and deposition by MOF-derived hierarchically ordered carbonaceous composite for high-energy lithium-sulfur batteries. *Adv. Funct. Mater.* 29, 1900875. doi:10.1002/adfm.201900875

Goodenough, J. B., and Park, K.-S. (2013). The li-ion rechargeable battery: a perspective. *J. Am. Chem. Soc.* 135, 1167–1176. doi:10.1021/ja3091438

Gu, X., Kang, H., Shao, C., Ren, X., and Liu, X. (2020). A typha angustifolia-like MoS_2/carbon nanofiber composite for high performance Li-S batteries. *Front. Chem.* 8, 149. doi:10.3389/fchem.2020.00149

Gu, X., and Lai, C. (2019). One dimensional nanostructures contribute better Li-S and Li-Se batteries: progress, challenges and perspectives. *Energy Storage Mater.* 23, 190–224. doi:10.1016/j.ensm.2019.05.013

Gu, X., Tang, T., Liu, X., and Hou, Y. (2019). Rechargeable metal batteries based on selenium cathodes: progress, challenges and perspectives. *J. Mater. Chem. A* 7, 11566–11583. doi:10.1039/c8ta12537f

Guo, Y., Xiao, J., Hou, Y., Wang, Z., and Jiang, A. (2017). Carbon nanotube doped active carbon coated separator for enhanced electrochemical performance of lithium-sulfur batteries. *J. Mater. Sci. Mater. Electron.* 28, 17453–17460. doi:10.1007/s10854-017-7679-7

He, Z., Jiang, Y., Wei, Y., Zhao, C., Jiang, F., Li, L., et al. (2018). N,P co-doped carbon microsphere as superior electrocatalyst for VO2+/VO2+ redox reaction. *Electrochim. Acta.* 259, 122–130. doi:10.1016/j.electacta.2017.10.169

Hong, X.-J., Tang, X.-Y., Wei, Q., Song, C.-L., Wang, S.-Y., Dong, R.-F., et al. (2018). Efficient encapsulation of small S2-4 molecules in MOF-derived flowerlike nitrogen-doped microporous carbon nanosheets for high-performance Li-S batteries. *ACS Appl. Mater. Interfaces.* 10, 9435–9443. doi:10.1021/acsami.7b19609

Hou, Y., Li, J., Gao, X., Wen, Z., Yuan, C., and Chen, J. (2016). 3D dual-confined sulfur encapsulated in porous carbon nanosheets and wrapped with graphene aerogels as a cathode for advanced lithium sulfur batteries. *Nanoscale* 8, 8228–8235. doi:10.1039/c5nr09037g

Huang, C., Zhou, Y., and Shu, H. (2020). Synergetic restriction to polysulfides by hollow $FePO_4$ nanospheres wrapped by reduced graphene oxide for lithium-sulfur battery. *Electrochimica Acta* 329, 135135.

Jiang, H., Liu, X.-C., Wu, Y., Shu, Y., Gong, X., Ke, F.-S., et al. (2018). Metal-organic frameworks for high charge-discharge rates in lithium-sulfur batteries. *Angew. Chem. Int. Ed.* 57, 3916–3921. doi:10.1002/anie.201712872

Kong, L., Li, B.-Q., Peng, H.-J., Zhang, R., Xie, J., Huang, J.-Q., et al. (2018). Porphyrin-derived graphene-based nanosheets enabling strong polysulfide chemisorption and rapid kinetics in lithium-sulfur batteries. *Adv. Energy Mater.* 8, 1800849. doi:10.1002/aenm.201800849

Leng, J., Wang, Z., Wang, J., Wu, H.-H., Yan, G., Li, X., et al. (2019). Advances in nanostructures fabricated via spray pyrolysis and their applications in energy storage and conversion. *Chem. Soc. Rev.* 48, 3015–3072. doi:10.1039/c8cs00904j

Li, G., Lei, W., Luo, D., Deng, Y., Deng, Z., Wang, D., et al. (2018). Stringed "tube on cube" nanohybrids as compact cathode matrix for high-loading and lean-electrolyte lithium-sulfur batteries. *Energy Environ. Sci.* 11, 2372–2381. doi:10.1039/c8ee01377b

Li, G., Sun, J., Hou, W., Jiang, S., Huang, Y., and Geng, J. (2016). Three-dimensional porous carbon composites containing high sulfur nanoparticle content for high-performance lithium-sulfur batteries. *Nat. Commun.* 7, 10601. doi:10.1038/ncomms10601

Lin, Y., Qiu, Z., Li, D., Ullah, S., Hai, Y., Xin, H., et al. (2018). NiS2@CoS2 nanocrystals encapsulated in N-doped carbon nanocubes for high performance lithium/sodium ion batteries. *Energy Storage Mater.* 11, 67–74. doi:10.1016/j.ensm.2017.06.001

Liu, X., Huang, J.-Q., Zhang, Q., and Mai, L. (2017). Nanostructured metal oxides and sulfides for lithium-sulfur batteries. *Adv. Mater.* 29, 1601759. doi:10.1002/adma.201601759

Ma, Z., Tao, L., Liu, D., Li, Z., Zhang, Y., Liu, Z., et al. (2017). Ultrafine nano-sulfur particles anchored on *in situ* exfoliated graphene for lithium-sulfur batteries. *J. Mater. Chem. A* 5, 9412–9417. doi:10.1039/c7ta01981e

Peng, H.-J., Huang, J.-Q., Cheng, X.-B., and Zhang, Q. (2017). Review on high-loading and high-energy lithium-sulfur batteries. *Adv. Energy Mater.* 7, 1700260. doi:10.1002/aenm.201700260

Qin, X., Wang, X., Sun, J., Lu, Q., Omar, A., and Mikhailova, D. (2020). Polypyrrole wrapped V(2)O(5) nanowires composite for advanced aqueous zinc-ion batteries. *Front Energy Res.* 8, 199. doi:10.3389/fenrg.2020.00199

Razzaq, A. A., Yao, Y. Z., Shah, R., Qi, P. W., Miao, L. X., Chen, M. Z., et al. (2019). High-performance lithium sulfur batteries enabled by a synergy between sulfur and carbon nanotubes. *Energy Storage Mater.* 16, 194–202. doi:10.1016/j.ensm.2018.05.006

Tang, Y., Zheng, S., Xu, Y., Xiao, X., Xue, H., and Pang, H. (2018). Advanced batteries based on manganese dioxide and its composites. *Energy Storage Mater.* 12, 284–309. doi:10.1016/j.ensm.2018.02.010

Tong, Z., Yang, R., Wu, S., Shen, D., Jiao, T., Zhang, K., et al. (2019). Surface-engineered black niobium Oxide@Graphene nanosheets for high-performance sodium-/potassium-ion full batteries. *Small* 15, 1901272. doi:10.1002/smll.201901272

Wang, B., Hu, C., and Dai, L. (2016). Functionalized carbon nanotubes and graphene-based materials for energy storage. *Chem. Commun.* 52, 14350–14360. doi:10.1039/c6cc05581h

Wang, X., Liu, Y., Zeng, J., Peng, C., and Wang, R. (2019). MoO2/C hollow nanospheres synthesized by solvothermal method as anode material for lithium-ion batteries. *Ionics* 25, 437–445. doi:10.1007/s11581-018-2765-2

Wang, Z., Dong, Y., Li, H., Zhao, Z., Wu, H. B., Hao, C., et al. (2014). Enhancing lithium-sulphur battery performance by strongly binding the discharge products on amino-functionalized reduced graphene oxide. *Nat. Commun.* 5, 5002. doi:10.1038/ncomms6002

Wu, F., Lv, H., Chen, S., Lorger, S., Srot, V., Oschatz, M., et al. (2019a). Natural vermiculite enables high-performance in lithium-sulfur batteries via electrical double layer effects. *Adv. Funct. Mater.* 29, 1902820. doi:10.1002/adfm.201902820

Wu, Y., Chen, J., Li, C., Li, F., Liu, K., Liu, H., et al. (2019b). Effect of *in-situ* doped anions on electrochemical performances of cathodically electrodeposited Ni(OH)2. *J. Phys. Chem. Solid.* 124, 352–360. doi:10.1016/j.jpcs.2018.05.050

Wu, L., Hu, Y., Zhang, X., Liu, J., Zhu, X., and Zhong, S. (2018). Synthesis of carbon-coated Na 2 MnPO 4 F hollow spheres as a potential cathode material for Na-ion batteries. *J. Power Sources.* 374, 40–47. doi:10.1016/j.jpowsour.2017.11.029

Xiao, D., Li, Q., Zhang, H., Ma, Y., Lu, C., Chen, C., et al. (2017). A sulfur host based on cobalt-graphitic carbon nanocages for high performance lithium-sulfur batteries. *J. Mater. Chem. A.* 5, 24901–24908. doi:10.1039/c7ta08483h

Xue, W., Yan, Q.-B., Xu, G., Suo, L., Chen, Y., Wang, C., et al. (2017). Double-oxide sulfur host for advanced lithium-sulfur batteries. *Nano Energy.* 38, 12–18. doi:10.1016/j.nanoen.2017.05.041

Yang, T., Yu, X., Liu, C., Liang, L., and Wang, W. (2018a). High-performance lithium storage properties based on molybdenum trioxide nanobelts. *Solid State Ion.* 326, 1–4. doi:10.1016/j.ssi.2018.09.002

Yang, W., Yang, W., Song, A., Sun, G., and Shao, G. (2018b). 3D interconnected porous carbon nanosheets/carbon nanotubes as a polysulfide reservoir for high performance lithium-sulfur batteries. *Nanoscale* 10, 816–824. doi:10.1039/c7nr06805k

Yang, Z., Yang, Y., Guo, H., Wang, Z., Li, X., Zhou, Y., et al. (2018c). Compact structured silicon/carbon composites as high-performance anodes for lithium ion batteries. *Ionics* 24, 3405–3411. doi:10.1007/s11581-018-2486-6

Yang, Y., Hou, H., Zou, G., Shi, W., Shuai, H., Li, J., et al. (2019). Electrochemical exfoliation of graphene-like two-dimensional nanomaterials. *Nanoscale* 11, 16–33. doi:10.1039/c8nr08227h

Ye, X., Lin, Z., Liang, S., Huang, X., Qiu, X., Qiu, Y., et al. (2019). Upcycling of electroplating sludge into ultrafine Sn@C nanorods with highly stable lithium storage performance. *Nano Lett.* 19, 1860–1866. doi:10.1021/acs.nanolett.8b04944

Yin, B., Cao, X., Pan, A., Luo, Z., Dinesh, S., Lin, J., et al. (2018). Encapsulation of CoS x nanocrystals into N/S Co-doped honeycomb-like 3D porous carbon for high-performance lithium storage. *Adv. Sci.* 5, 1800829. doi:10.1002/advs.201800829

Yuan, H., Chen, X. L., Zhou, G. M., Zhang, W. K., Luo, J. M., Huang, H., et al. (2017). Efficient activation of Li2S by transition metal phosphides nanoparticles for highly stable lithium-sulfur batteries. *ACS Energy Lett.* 2, 1711–1719. doi:10.1021/acsenergylett.7b00465

Yuan, H., Zhang, W., Wang, J.-g., Zhou, G., Zhuang, Z., Luo, J., et al. (2018). Facilitation of sulfur evolution reaction by pyridinic nitrogen doped carbon nanoflakes for highly-stable lithium-sulfur batteries. *Energy Storage Mater.* 10, 1–9. doi:10.1016/j.ensm.2017.07.015

Yuan, Z., Peng, H.-J., Hou, T.-Z., Huang, J.-Q., Chen, C.-M., Wang, D.-W., et al. (2016). Powering lithium-sulfur battery performance by propelling polysulfide redox at sulfiphilic hosts. *Nano Lett.* 16, 519–527. doi:10.1021/acs.nanolett.5b04166

Zeng, J. H., Wang, Y. F., Gou, S. Q., Zhang, L. P., Chen, Y., Jiang, J. X., et al. (2017). Sulfur in hyper-cross-linked porous polymer as cathode in lithium-sulfur batteries with enhanced electrochemical properties. *ACS Appl. Mater. Interfaces.* 9, 34783–34792. doi:10.1021/acsami.7b07982

Zhang, L., Wu, C., Liu, J., Zhao, X. N., Wang, Z. Q., Xu, H. Y., et al. (2018). The nature of lithium-ion transport in low power consumption $LiFePO_4$ resistive memory with graphite as electrode. *Phys. Status Solidi Rapid Res. Lett.* 12, , 2018 1800320. doi:10.1002/pssr.201870333

Zhang, Q., Qiao, Z., Cao, X., Qu, B., Yuan, J., Fan, T.-E., et al. (2020). Rational integration of spatial confinement and polysulfide conversion catalysts for high sulfur loading lithium-sulfur batteries. *Nanoscale Horiz.* 5, 720–729. doi:10.1039/c9nh00663j

Zhang, Y., Heim, F. M., Song, N., Bartlett, J. L., and Li, X. (2017). New insights into mossy Li induced anode degradation and its formation mechanism in Li-S batteries. *ACS Energy Lett.* 2, 2696–2705. doi:10.1021/acsenergylett.7b00886

Zhao, B., Zhang, L., Zhang, Q., Chen, D., Cheng, Y., Deng, X., et al. (2018). Rational design of nickel hydroxide-based nanocrystals on graphene for ultrafast energy storage. *Adv. Energy Mater.* 8, 1702247. doi:10.1002/aenm.201702247

Zheng, C., Niu, S., Lv, W., Zhou, G., Li, J., Fan, S., et al. (2017). Propelling polysulfides transformation for high-rate and long-life lithium-sulfur batteries. *Nano Energy.* 33, 306–312. doi:10.1016/j.nanoen.2017.01.040

Zhu, K., Wang, C., Chi, Z., Ke, F., Yang, Y., Wang, A., et al. (2019). How far away are lithium-sulfur batteries from commercialization? *Front Energy Res.* 7, 123. doi:10.3389/fenrg.2019.00123